Spline-based Spectrum Cartography for Cognitive Radios

Gonzalo Mateos, Juan-Andrés Bazerque, and Georgios B. Giannakis (contact author)
Dept. of ECE, University of Minnesota
200 Union St. SE, Minneapolis, MN 55455, USA
Emails: {mate0058,bazer002,georgios}@ece.umn.edu

***Abstract*—A cooperative approach to the sensing task of wireless cognitive radio (CR) networks is introduced based on a spatial model of the power spectrum density (PSD). The model entails a basis expansion of the PSD in frequency, weighted by unknown spatial functions that are estimated from CR measurements. A novel model estimator is developed using a least-squares (LS) criterion regularized with a smoothing penalty. The estimator yields a finitely-parameterized two-dimensional surface spanned by thin-plate splines, which approximates the distribution of power in space. An online PSD tracker is also developed for slowly time-varying power spectra. Different from existing approaches to interference spectrum cartography, the novel sensing scheme neither requires knowledge of second-order spatial statistics, nor it relies on stationarity assumptions.**

I. Introduction

Spectrum sensing is of paramount importance to the operation of CR systems, which aim at efficient spectrum utilization. Sensing the ambient interference spectrum enables spatial frequency reuse and allows for dynamic spectrum allocation. Energy detection is a simple yet effective scheme that has been widely adopted to this end, because it circumvents the need for synchronization with unknown transmitted signals; see, e.g., [5], [7] and references therein. Collaboration among CRs can markedly improve the sensing performance [9], and is key to revealing opportunities for spatial frequency reuse [8].

This paper develops a collaborative sensing scheme whereby receiving CRs cooperate to estimate the distribution of power in space $\boldsymbol{x}$ and frequency f, namely the spectrum map $\Phi(\boldsymbol{x}, f)$. Knowing the spectrum at any location allows remote CRs to reuse dynamically idle bands. It also enables CRs to adapt their transmit-power so as to minimally interfere with licensed transmitters. In this context, the threshold for deciding occupancy of a frequency band is not set according to the probability of false alarms, but through comparing PSD estimates against prescribed power levels.

A related approach was taken in [1], where interference measurements are spatially interpolated using the Kriging technique to obtain the desired $\Phi(\boldsymbol{x}, f)$. This method is applicable provided that the CR observations are spatially wide-sense stationary, and requires knowledge of the mean and auto-covariance of the spatial random field. However, obtaining accurate statistical models to characterize the radio environment is challenging [10].

The present paper introduces a novel PSD estimator, which is obtained by fitting a space-frequency model to (time-averaged) periodogram measurements collected at spatially dispersed CRs. The estimator need not be extremely accurate, but precise enough to identify spectrum holes. This motivates adopting a basis expansion to model the PSD dependence in frequency. As far as the spatial dependence is concerned, the model must account for path loss, fading, mobility, and shadowing effects, all of which vary with the propagation medium. For this reason, it is prudent to let the data dictate the spatial component of the model. This becomes possible through a regularized least-squares (LS) criterion, which effects spatial smoothness in the estimated PSD. In a nutshell, the novel model for $\Phi(\boldsymbol{x}, f)$ entails a preselected basis in frequency and spline kernels in the spatial dimension. An online version of the novel scheme is also developed to track slow variations in the PSD map across time, a feature that is particularly useful when e.g., a transmitter joins or departs.

The spline-based PSD estimator here provides an alternative to [2], where basis expansions are used both in space and frequency. Different from [1], [2], it does not require a spatial covariance model or pathloss law chosen a fortiori. Moreover, it captures general propagation characteristics including both shadowing and fading. Similar to [2] though, the resultant algorithms work as general field estimation and localization tools.

II. Spatial PSD Model

Consider a set of N_s sources transmitting signals $\{u_s(t)\}_{s=1}^{N_s}$ using portions of the overall bandwidth B. The objective of revealing which of these portions (sub-bands) are available for new systems to transmit, suggests that the PSD estimate sought does not need to be super accurate. This motivates modeling the PSD of each $u_s(t)$ as

$$\Phi_s(f) = \sum_{\nu=1}^{N_b} \theta_{s\nu} b_\nu(f), \quad s = 1, \ldots, N_s \tag{1}$$

where the basis $b_\nu(f)$ is centered at frequency f_ν, $\nu = 1, \ldots, N_b$. The example depicted in Fig. 1 involves overlap-

† Work in this paper was supported by the USDoD ARO Grant No. W911NF-05-1-0283; and also through collaborative participation in the C&N Consortium sponsored by the U. S. ARL under the CTA Program, Cooperative Agreement DAAD19-01-2-0011. The U. S. Government is authorized to reproduce and distribute reprints for Government purposes notwithstanding any copyright notation thereon.

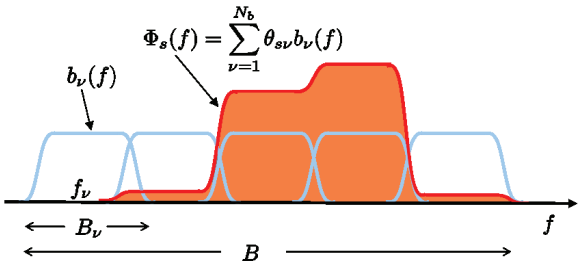

Fig. 1. Expansion with overlapping raised cosine pulses.

ping raised cosine bases of unit height and support $B_\nu = [f_\nu - (1+\rho)/2T_s, f_\nu + (1+\rho)/2T_s]$, where T_s is the symbol period and ρ stands for the roll-off factor. Such bases can model transmit spectra of e.g., multicarrier systems. In other situations, power spectral masks may dictate sharp transitions between contiguous sub-bands, cases in which non-overlapping rectangular bases may be more appropriate. All in all, the set of bases should be selected to accommodate a priori knowledge about the PSD.

The power transmitted by source s will propagate to the location $\boldsymbol{x} \in \mathbb{R}^2$ according to a generally unknown spatial loss function $l_s(\boldsymbol{x}) : \mathbb{R}^2 \to \mathbb{R}$. As a result, the contribution of source s to the PSD at point $\boldsymbol{x}$ is $l_s(\boldsymbol{x}) \sum_{\nu=1}^{N_b} \theta_{s\nu} b_\nu(f)$; and the PSD due to all sources received at $\boldsymbol{x}$ will be given by $\Phi(\boldsymbol{x}, f) = \sum_{s=1}^{N_s} l_s(\boldsymbol{x}) \sum_{\nu=1}^{N_b} \theta_{s\nu} b_\nu(f)$. Such a model can be simplified by defining the function $g_\nu(\boldsymbol{x}) := \sum_{s=1}^{N_s} \theta_{s\nu} l_s(\boldsymbol{x})$. With this definition and upon exchanging the order of summation, the spatial PSD model is

$$\Phi(\boldsymbol{x}, f) = \sum_{\nu=1}^{N_b} g_\nu(\boldsymbol{x}) b_\nu(f) \tag{2}$$

where functions $\{g_\nu(\boldsymbol{x})\}_{\nu=1}^{N_b}$ are to be estimated. They represent the aggregate distribution of power across space corresponding to the frequencies spanned by the bases $\{b_\nu\}$. Observe that the sources are not explicitly present in (2). Even if this model could have been postulated directly, the previous discussion justifies the factorization of the power spectral map per band in factors depending on each variable $\boldsymbol{x}$ and f.

III. Cooperative PSD estimation

The sensing strategy will rely on the periodogram estimate $\widehat{\phi}_{rn}(\tau)$ at a set of receiving (sampling) locations $\mathcal{X} := \{\boldsymbol{x}_r\}_{r=1}^{N_r} \in \mathbb{R}^2$, frequencies $\mathcal{F} := \{f_n\}_{n=1}^{N} \in B$, and time-slots $\{\tau\}_{\tau=1}^{T}$. In order to reduce the variance of the periodogram and mitigate fading effects, $\widehat{\phi}_{rn}(\tau)$ is averaged across a window of T time-slots, to obtain

$$\varphi_{rn} := \frac{1}{T} \sum_{\tau=1}^{T} \widehat{\phi}_{rn}(\tau). \tag{3}$$

Hence, the envisioned setup consists of N_r receiving CRs, which collaborate to build the PSD map based on PSD observations $\{\varphi_{rn}\}$. The bulk of processing is performed centrally at a fusion center (FC), which is assumed to know the locations $\mathcal{X}$ of all CRs and the sensed tones in $\mathcal{F}$. The FC receives – over a dedicated control channel – the vector of samples $\boldsymbol{\varphi}_r := [\varphi_{r1} \ldots \varphi_{rN}]' \in \mathbb{R}^N$ taken by node r for all $r = 1, \ldots, N_r$, where $'$ denotes transposition.

While a basis expansion model can be introduced for the spatial loss function $l_s(\boldsymbol{x})$ as well [2], the uncertainty on the location of the sources and obstructions may render such a model imprecise. This will happen, e.g., when shadowing is present. The alternative approach followed here relies on estimation of the functions $g_\nu(\boldsymbol{x})$ based on the data $\{\varphi_{rn}\}$. To capture the smooth portions of $\Phi(\boldsymbol{x}, f)$, the criterion for selecting $g_\nu(\boldsymbol{x})$ will be regularized using a so termed thin-plate penalty [12, p. 30]. This penalty extends to $\mathbb{R}^2$ the one-dimensional roughness regularization used in smoothing spline models. Accordingly, $\{g_\nu\}_{\nu=1}^{N_b}$ is estimated as

$$\{\hat{g}_\nu\}_{\nu=1}^{N_b} := \arg\min_{\{g_\nu \in \mathcal{S}\}} \frac{1}{\tilde{N}} \sum_{r=1}^{N_r} \sum_{n=1}^{N} \left(\varphi_{rn} - \sum_{\nu=1}^{N_b} g_\nu(\boldsymbol{x}_r) b_\nu(f_n) \right)^2 + \lambda \sum_{\nu=1}^{N_b} \int_{\mathbb{R}^2} ||\nabla^2 g_\nu(\boldsymbol{x})||_F^2 d\boldsymbol{x} \tag{4}$$

where $\tilde{N} := N_r N$, and $||\nabla^2 g_\nu||_F$ denotes the Frobenius norm of the Hessian of g_ν. The optimization is over $\mathcal{S}$, the space of Sobolev functions, for which the penalty is well defined [4]. The parameter $\lambda \geq 0$ controls the degree of smoothing. Specifically, for $\lambda = 0$ the estimates in (4) correspond to *rough* functions interpolating the data; while as $\lambda \to \infty$ the estimates must be linear functions (cf. $\nabla^2 \hat{g}_\nu(\boldsymbol{x}) \equiv \mathbf{0}$). A smoothing parameter in between these limiting values will be selected using a leave-one-out cross-validation approach as in e.g., [12].

A. The thin-plate splines solution

The optimization problem (4) is variational in nature, and in principle requires searching over the infinite-dimensional functional space $\mathcal{S}$. Interestingly, it will turn out that (4) admits closed-form, finite-dimensional minimizers $\hat{g}_\nu(\boldsymbol{x})$. This should not be surprising when the bases $b_\nu(f)$ have non-overlapping support because (4) decouples per $g_\nu(\boldsymbol{x})$. Indeed, under this condition on the bases (4) can be reformulated as

$$\begin{aligned} \{\hat{g}_\nu\} &= \arg\min_{\{g_\nu \in \mathcal{S}\}} \sum_{\nu=1}^{N_b} \left[\frac{1}{\tilde{N}} \sum_{r=1}^{N_r} \left(\tilde{\varphi}_{r\nu} - \tilde{b}_\nu g_\nu(\boldsymbol{x}_r) \right)^2 + \lambda \int_{\mathbb{R}^2} ||\nabla^2 g_\nu(\boldsymbol{x})||_F^2 d\boldsymbol{x} \right] \\ &= \left\{ \arg\min_{g_\nu \in \mathcal{S}} \frac{1}{\tilde{N}} \sum_{r=1}^{N_r} \left(\tilde{\varphi}_{r\nu} - \tilde{b}_\nu g_\nu(\boldsymbol{x}_r) \right)^2 + \lambda \int_{\mathbb{R}^2} ||\nabla^2 g_\nu(\boldsymbol{x})||_F^2 d\boldsymbol{x} \right\} \end{aligned} \tag{5}$$

where $\tilde{\varphi}_{r\nu} := \sum_{n: f_n \in B_\nu} \varphi_{rn}$ and $\tilde{b}_\nu := \sum_{n: f_n \in B_\nu} b_\nu(f_n)$. Thus, each $\hat{g}_\nu(\boldsymbol{x})$ can be obtained separately by solving the standard thin-plate splines problem inside the curly brackets in (5); see also [12, p. 31]. For the general case however, (4) does not exhibit a separable structure, and the following result

provides a generalization to the standard multi-dimensional spline models.

Proposition 1: *The estimates* $\{\hat{g}_\nu\}_{\nu=1}^{N_b}$ *in* (4) *are thin-plate splines expressible in closed form as*

$$\hat{g}_\nu(\boldsymbol{x}) = \sum_{r=1}^{N_r} \beta_{\nu r} K(||\boldsymbol{x} - \boldsymbol{x}_r||_2) + \boldsymbol{\alpha}'_{\nu 1}\boldsymbol{x} + \alpha_{\nu 0} \qquad (6)$$

where $K(\rho) := \rho^2 \log(\rho)$ *and* $\boldsymbol{\beta}_\nu := [\beta_{\nu 1} \dots \beta_{\nu N_r}]'$ *is constrained to the linear subspace* $\mathcal{B} := \{\boldsymbol{\beta} \in \mathbb{R}^{N_r} : \sum_{r=1}^{N_r} \beta_r = 0, \sum_{r=1}^{N_r} \beta_r \boldsymbol{x}_r = \mathbf{0},\ \boldsymbol{x}_r \in \mathcal{X}\}$ *for* $\nu = 1, \dots, N_b$.

Proof: See [3, Proof of Proposition 1]. ■

Remark 1: Proposition 1 asserts that the model in (2) can afford overlapping frequency bases combined with spatial splines, which allow for finite parametrization of the PSD map [cf. (6)]. This is particularly important for non-FDMA based CR networks.

What is left to determine are the coefficients $\{\boldsymbol{\beta}_\nu, \boldsymbol{\alpha}_{\nu 1}, \alpha_{\nu 0}\}_{\nu=1}^{N_b}$, the subject dealt with next.

B. Optimum coefficients: existence and uniqueness

Consider the vector $\boldsymbol{\varphi}_n := [\varphi_{1n} \dots \varphi_{N_r n}]'$ of averaged periodogram samples taken at frequency f_n, and form the supervector of all network-wide observations $\boldsymbol{\varphi} := [\boldsymbol{\varphi}'_1 \dots \boldsymbol{\varphi}'_N]' \in \mathbb{R}^{\tilde{N}}$. For all $\nu = 1, \dots, N_b$, define $\boldsymbol{\alpha}_\nu := [\alpha_{\nu 0}\ \boldsymbol{\alpha}'_{\nu 1}]' \in \mathbb{R}^3$ and recall that $\boldsymbol{\beta}_\nu := [\beta_{\nu 1} \dots \beta_{\nu N_r}]'$. Then, form the respective supervectors $\boldsymbol{\alpha} := [\boldsymbol{\alpha}'_1 \dots \boldsymbol{\alpha}'_{N_b}]' \in \mathbb{R}^{3N_b}$ and $\boldsymbol{\beta} := [\boldsymbol{\beta}'_1 \dots \boldsymbol{\beta}'_{N_b}]' \in \mathbb{R}^{N_r N_b}$. Finally, introduce three matrices: i) $\mathbf{T} \in \mathbb{R}^{N_r \times 3}$ with rth row $\mathbf{t}'_r := [1\ \boldsymbol{x}'_r]$ for $r = 1, \dots, N_r$ and $\boldsymbol{x}_r \in \mathcal{X}$; ii) $\mathbf{B} \in \mathbb{R}^{N \times N_b}$ with nth row $\mathbf{b}'_n := [b_1(f_n) \dots b_{N_b}(f_n)]$ for $n = 1, \dots, N$; and iii) $\mathbf{K} \in \mathbb{R}^{N_r \times N_r}$ with ij-th entry $[\mathbf{K}]_{ij} := K(||\boldsymbol{x}_i - \boldsymbol{x}_j||)$ for $\boldsymbol{x}_i, \boldsymbol{x}_j \in \mathcal{X}$.

Using the previous definitions, observe that the constraints $\boldsymbol{\beta}_\nu \in \mathcal{B}$ in Proposition 1 can be expressed as $\mathbf{T}'\boldsymbol{\beta}_\nu = \mathbf{0}$ for each $\nu = 1, \dots, N_b$, or jointly as $(\mathbf{I}_{N_b} \otimes \mathbf{T}')\boldsymbol{\beta} = \mathbf{0}$, where $\otimes$ denotes Kronecker product and $\mathbf{I}_{N_b}$ stands for the identity matrix of size $N_b \times N_b$. Upon plugging (6) in (4), it is shown in the Appendix that the optimal coefficients $\{\hat{\boldsymbol{\alpha}}, \hat{\boldsymbol{\beta}}\}$ defining $\{\hat{g}_\nu(\boldsymbol{x})\}_{\nu=1}^{N_b}$ are obtained as solutions to the following constrained, regularized LS problem

$$\min_{\boldsymbol{\alpha},\boldsymbol{\beta}} \frac{1}{\tilde{N}} \|\boldsymbol{\varphi} - (\mathbf{B} \otimes \boldsymbol{K})\boldsymbol{\beta} - (\mathbf{B} \otimes \mathbf{T})\boldsymbol{\alpha}\|_2^2 + \lambda \boldsymbol{\beta}'(\mathbf{I}_{N_b} \otimes \mathbf{K})\boldsymbol{\beta}$$
$$\text{s. t.} \quad (\mathbf{I}_{N_b} \otimes \mathbf{T}')\boldsymbol{\beta} = \mathbf{0}. \qquad (7)$$

Even though $\mathbf{K}$ (hence $\mathbf{I}_{N_b} \otimes \mathbf{K}$) is not positive definite, it is still possible to show that $\boldsymbol{\beta}'(\mathbf{I}_{N_b} \otimes \mathbf{K})\boldsymbol{\beta} > 0$ for any $\boldsymbol{\beta}$ such that $(\mathbf{I}_{N_b} \otimes \mathbf{T}')\boldsymbol{\beta} = \mathbf{0}$ [4], implying that (7) is convex. To find $\{\hat{\boldsymbol{\alpha}}, \hat{\boldsymbol{\beta}}\}$ introduce the QR decompositions of $\mathbf{T}$ and $\mathbf{B}$

$$\mathbf{T} = [\mathbf{Q}_1\ \mathbf{Q}_2] \begin{bmatrix} \mathbf{R} \\ \mathbf{0} \end{bmatrix}, \quad \mathbf{B} = [\boldsymbol{\Omega}_1\ \boldsymbol{\Omega}_2] \begin{bmatrix} \boldsymbol{\Gamma} \\ \mathbf{0} \end{bmatrix} \qquad (8)$$

where $[\mathbf{Q}_1\ \mathbf{Q}_2]$ and $[\boldsymbol{\Omega}_1\ \boldsymbol{\Omega}_2]$ are orthogonal, while $\mathbf{R}$ and $\boldsymbol{\Gamma}$ are upper triangular. Proceeding along the lines of [12, p. 33], note first that the constraint $(\mathbf{I}_{N_b} \otimes \mathbf{T}')\boldsymbol{\beta} = \mathbf{0}$ implies the existence of $\boldsymbol{\gamma} \in \mathbb{R}^{N_b(N_r-3)}$ satisfying $\boldsymbol{\beta} = (\mathbf{I}_{N_b} \otimes \mathbf{Q}_2)\boldsymbol{\gamma}$. Hence, $\{\hat{\boldsymbol{\alpha}}, \hat{\boldsymbol{\beta}}\}$ can be obtained by solving the following system of linear equations

$$(\mathbf{B} \otimes \mathbf{Q}'_2)\boldsymbol{\varphi} = \left[(\mathbf{B}'\mathbf{B} \otimes \mathbf{Q}'_2\mathbf{K}\mathbf{Q}_2) + \tilde{N}\lambda \mathbf{I}_{N_b(N_r-3)}\right] \hat{\boldsymbol{\gamma}} \quad (9)$$

$$[\boldsymbol{\Gamma} \otimes \mathbf{R}]\hat{\boldsymbol{\alpha}} = (\boldsymbol{\Omega}'_1 \otimes \mathbf{Q}'_1)\boldsymbol{\varphi} - (\boldsymbol{\Gamma} \otimes \mathbf{Q}'_1\mathbf{K}\mathbf{Q}_2)\hat{\boldsymbol{\gamma}} \qquad (10)$$

$$\hat{\boldsymbol{\beta}} = (\mathbf{I}_{N_b} \otimes \mathbf{Q}_2)\hat{\boldsymbol{\gamma}}. \qquad (11)$$

Matrix $\mathbf{Q}'_2\mathbf{K}\mathbf{Q}_2$ is positive definite and $\text{rank}(\boldsymbol{\Gamma} \otimes \mathbf{R}) = \text{rank}(\boldsymbol{\Gamma})\text{rank}(\mathbf{R})$; see e.g., [6]. It thus follows from (9)-(10) that (7) admits a unique solution if and only if $\boldsymbol{\Gamma}$ and $\mathbf{R}$ are invertible (correspondingly, $\mathbf{B}$ and $\mathbf{T}$ have full column rank). These conditions place practical constraints that should be taken into account at the system design stage. Specifically, $\mathbf{T}$ has full column rank if and only if the points in $\mathcal{X}$, i.e., the CR locations, are not aligned. Furthermore, $\mathbf{B}$ will have linearly independent columns provided the bases $\{b_\nu(f)\}_{\nu=1}^{N_b}$ comprise a linearly independent and complete set, i.e., $B \subseteq \bigcup_\nu B_\nu$. Note that completeness precludes all frequencies $\{f_n\}_{n=1}^{N}$ from falling outside the aggregate support of the basis set, hence leading to undesired all-zero columns in $\mathbf{B}$.

Remark 2: The condition on $\mathcal{X}$ does not introduce an actual limitation as it can be easily satisfied in practice, especially when the CRs are randomly deployed. Likewise, the basis set is part of the system design and can be chosen to satisfy the conditions on $\mathbf{B}$.

The combined results in this section can be summarized in the following steps developed to estimate $\Phi(\boldsymbol{x}, f)$:

S1. Given $\boldsymbol{\varphi}$, solve (9)-(11) for $\hat{\boldsymbol{\alpha}}, \hat{\boldsymbol{\beta}}$.
S2. Substitute $\hat{\boldsymbol{\alpha}}, \hat{\boldsymbol{\beta}}$ in (6) to obtain $\{\hat{g}_\nu(\boldsymbol{x})\}_{\nu=1}^{N_b}$.
S3. Plug $\{\hat{g}_\nu(\boldsymbol{x})\}_{\nu=1}^{N_b}$ in (2) to estimate $\Phi(\boldsymbol{x}, f)$.

IV. Online PSD tracker

The real-time requirements on the sensing radios and the convenience of an estimator that adapts to changes in the spectrum map are the motivating reasons behind the online PSD tracker introduced in this section. The spectrum map estimator will be henceforth denoted by $\Phi(\boldsymbol{x}, f, \tau)$, to make its time dependence explicit.

Define the vector $\widehat{\boldsymbol{\phi}}_n(\tau) := [\widehat{\phi}_{1n}(\tau) \dots \widehat{\phi}_{N_r n}(\tau)]'$ of periodogram samples taken at frequency f_n by all CRs, and form the supervector $\widehat{\boldsymbol{\phi}}(\tau) := [\widehat{\boldsymbol{\phi}}'_1(\tau) \dots \widehat{\boldsymbol{\phi}}'_N(\tau)]' \in \mathbb{R}^{N_r N}$. Per time-slot $\tau = 1, 2, \dots$, the periodogram $\widehat{\boldsymbol{\phi}}(\tau)$ is averaged using the following adaptive counterpart of (3):

$$\boldsymbol{\varphi}(\tau) := \sum_{\tau'=1}^{\tau} \delta^{\tau - \tau'} \widehat{\boldsymbol{\phi}}(\tau') = \delta \boldsymbol{\varphi}(\tau - 1) + \widehat{\boldsymbol{\phi}}(\tau) \qquad (12)$$

which implements an exponentially weighted moving average (EWMA) operation with forgetting factor $\delta \in (0, 1)$. For every τ, the online estimator $\Phi(\boldsymbol{x}, f, \tau)$ is obtained by plugging in (2) the solution $\{\hat{g}_\nu(\boldsymbol{x}, \tau)\}_{\nu=1}^{N_b}$ of (4), after replacing φ_{rn} with $\varphi_{rn}(\tau)$ [cf. the entries of the vector in (12)]. In addition to mitigating fading effects, this adaptive approach can track slowly time-varying PSDs because the EWMA in (12) exponentially discards past data.

Suppose that per time-slot τ, the FC receives raw periodogram samples $\widehat{\boldsymbol{\phi}}(\tau)$ from the CRs in order to update

$\Phi(\boldsymbol{x}, f, \tau)$. The results of Section III apply for every τ, meaning that the $\{\hat{g}_\nu(\boldsymbol{x}, \tau)\}_{\nu=1}^{N_b}$ are given by (6), while the optimum coefficients $\{\hat{\boldsymbol{\alpha}}(\tau), \hat{\boldsymbol{\beta}}(\tau)\}$ are found after solving (9)-(11). Capitalizing on (12), straightforward manipulations in (9)-(11) show that $\{\hat{\boldsymbol{\alpha}}(\tau), \hat{\boldsymbol{\beta}}(\tau)\}$ are recursively given for all $\tau \geq 1$ by

$$\hat{\boldsymbol{\beta}}(\tau) = \delta\hat{\boldsymbol{\beta}}(\tau-1) + (\mathbf{I}_{N_b} \otimes \mathbf{Q}_2)\mathbf{G}_1\widehat{\boldsymbol{\phi}}(\tau) \quad (13)$$

$$\hat{\boldsymbol{\alpha}}(\tau) = \delta\hat{\boldsymbol{\alpha}}(\tau-1) + \mathbf{G}_2\widehat{\boldsymbol{\phi}}(\tau) \quad (14)$$

where the *time-invariant* matrices $\mathbf{G}_1$ and $\mathbf{G}_2$ are

$$\mathbf{G}_1 := \left[(\mathbf{B}'\mathbf{B} \otimes \mathbf{Q}_2'\mathbf{K}\mathbf{Q}_2) + \tilde{N}\lambda\mathbf{I}_{N_b(N_r-3)}\right]^{-1}(\mathbf{B} \otimes \mathbf{Q}_2')$$

$$\mathbf{G}_2 := [\boldsymbol{\Gamma} \otimes \mathbf{R}]^{-1}\left[(\boldsymbol{\Omega}_1' \otimes \mathbf{Q}_1') - (\boldsymbol{\Gamma} \otimes \mathbf{Q}_1'\mathbf{K}\mathbf{Q}_2)\mathbf{G}_1\right].$$

Recursions (13)-(14) provide a means to update $\Phi(\boldsymbol{x}, f, \tau)$ sequentially in time, by incorporating the newly acquired data from the CRs in $\widehat{\boldsymbol{\phi}}(\tau)$. There is no need to separately update $\boldsymbol{\varphi}(\tau)$ as in (12), yet the desired averaging takes place. Furthermore, matrices $\mathbf{G}_1$ and $\mathbf{G}_2$ need to be computed only once, during the startup phase of the network.

V. Numerical tests

Consider a set of $N_r = 100$ CRs uniformly distributed in an area of 1Km^2, cooperating to estimate the PSD map generated by $N_s = 5$ licensed users (sources) located as in Fig. 2. The transmitted signals are raised cosine pulses with roll-off factor $\rho = 0.5$, symbol period $T_s = 50$ms, and center frequency $f_s = 90 + 20s$MHz, $s = 1, \ldots, N_s$. All source signals have power $20W$, and overlap in the frequency band $B = [100, 300]$MHz (see the bases in Fig. 1). The PSD generated by source s experiences fading and shadowing effects in its propagation from $\boldsymbol{x}_s$ to any location $\boldsymbol{x}$, where it can be measured in the presence of noise. A 6-tap Rayleigh model is adopted for the multipath channel $H_s(f, \tau, \boldsymbol{x})$ between $\boldsymbol{x}_s$ and $\boldsymbol{x}$, whose mean adheres to the path-loss law $E(H_s) = \exp(-||\boldsymbol{x}_s - \boldsymbol{x}||_2^2/\Delta^2)$ with $\Delta = 0.8$. A deterministic shadowing effect is generated by a 18m-high and 500m-wide wall represented by the white segment in Fig. 2. It produces a knife-edge effect on the power emitted by the antennas at a height of 20m. The simulated tests presented here account for the shadowing at ground level. The additive Gaussian noise is assumed white in space and frequency with -10dB of variance compared to the average transmitter power received by the set of N_r radios.

A. Batch spectrum cartography

For $\tau = 1, \ldots, 500$, each radio computes the periodogram at $N = 16$ frequencies and updates the sample mean φ_{rn}, $n = 1, \ldots, N$ as in (3). These network-wide observations at $T = 500$ are collected in $\boldsymbol{\varphi}$, and upon following the steps at the end of Section III the spectrum map becomes available. This map is averaged across frequencies. Fig. 2 shows the position of the sources revealed, as well as the radially decaying spectra of four of them which are not affected by the obstacle. It also identifies the effect of the wall by flattening the spectrum emitted by the fifth source at the top-left corner.

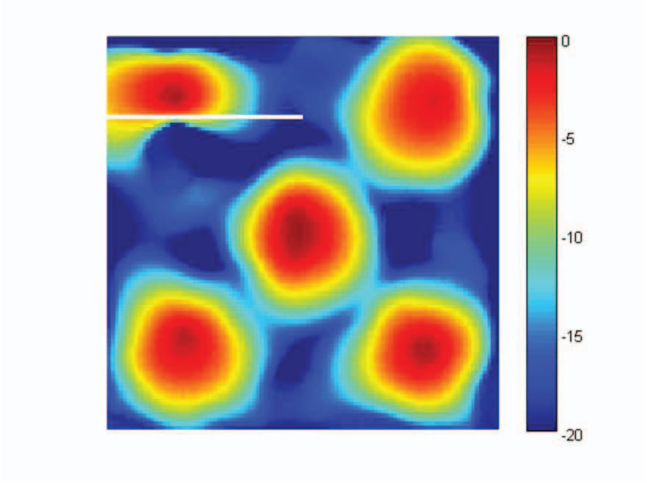

Fig. 2. Spectral map estimate in dB.

For simplicity, the frequency bases $b_\nu(f)$ were selected for this simulation as $N_b = 5$ raised cosine pulses coinciding with the actual transmitted PSDs. The smoothing parameter λ was chosen using the leave-one-out cross-validation approach [12], yielding the optimal tradeoff as dictated by the data. It effects smoothness which translates to congruence among PSD samples, allowing the radios to recover the radial aspect of the transmitted power. On the other hand, it compromises the sharp transition on the obstacle as the estimated PSD map shows a glitch at the south-west of the wall.

B. Tracking a transmitter's departure

The online estimator presented in Section IV is run for $\tau = 1, \ldots, 650$. Per time-slot τ, the CRs compute $\hat{\boldsymbol{\phi}}(\tau)$ and the new coefficients $\hat{\boldsymbol{\alpha}}(\tau)$ and $\hat{\boldsymbol{\beta}}(\tau)$ are updated using (14) and (13) respectively, with $\delta = 0.99$. In order to illustrate the PSD tracker, the transmitter at the center of Fig. 2 is shut-off at $\tau = 400$, and the PSD is estimated at that location. The result is shown in Fig. 3, where the solution is averaged across frequencies, and the error relative to the true model is presented. It shows that the estimator evolves toward the true value up to an error below -20dB, and that it is capable to adapt to the departing source. Specifically, three different periods are observed. When $\tau \in [0, 200)$, the error in $\Phi(\boldsymbol{x}, f, \tau)$ decreases because the recursive estimates in (14) and (13) improve thanks to averaging [cf. (12)]. When $\tau \in [200, 400)$, the estimator reaches steady state because the effective average window is elapsed, and new measurements do not add extra information. After $\tau = 400$, the radios around the central transmitter measure zero power, but the EWMA slowly forgets previous values; hence, the jump in the estimation error followed by the exponentially decaying trend.

VI. Concluding Remarks

A cooperative splines-based approach to spectrum cartography was developed for CR sensing. Simulated experiments

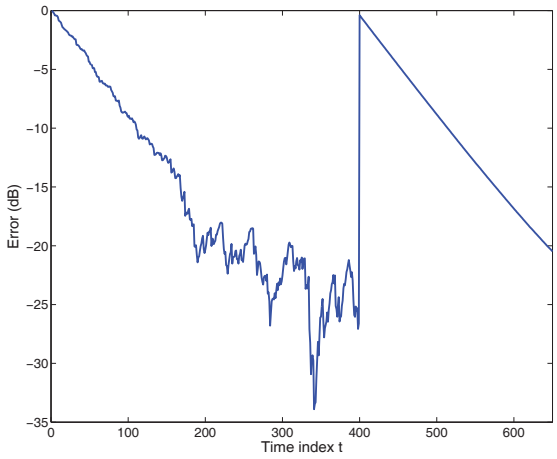

Fig. 3. Error evolution of tracking estimate in dB.

corroborate that the proposed estimator is effective in estimating the PSD generated by a set of sources in the presence of fading and shadowing. It can further track changes due to the departure of a transmitter.

The novel model and its estimation can be used in more general statistical inference, field estimation and localization problems, whenever the data admit a basis expansion over a proper subset of its dimensions. Furthermore, Proposition 1 extends to other kernels beyond splines, when the smoothing penalty is replaced by a norm induced from a reproducing kernel Hilbert space [12]. Also of interest is to quantify the number of sensors required to attain a prescribed approximation error, in light of the existing connections between spline-based reconstruction and Shannon's sampling theory [11].[1]

APPENDIX

Note from (6) that $\hat{g}_\nu(\boldsymbol{x}_r) = \mathbf{k}_r'\boldsymbol{\beta}_\nu + \mathbf{t}_r'\boldsymbol{\alpha}_\nu$, where $\mathbf{k}_r'$ and $\mathbf{t}_r'$ are the rth rows of $\mathbf{K}$ and $\mathbf{T}$, respectively. The first term in the cost of (4) can be expressed as (up to a factor $\tilde{N}^{-1}$)

$$\begin{aligned}
&\sum_{n=1}^{N}\sum_{r=1}^{N_r}\left(\varphi_{rn} - \sum_{\nu=1}^{N_b} b_\nu(f_n)[\mathbf{k}_r'\boldsymbol{\beta}_\nu + \mathbf{t}_r'\boldsymbol{\alpha}_\nu]\right)^2 \\
&\quad = \sum_{n=1}^{N}\sum_{r=1}^{N_r}\left(\varphi_{rn} - (\mathbf{b}_n\otimes\mathbf{k}_r)'\boldsymbol{\beta} - (\mathbf{b}_n\otimes\mathbf{t}_r)'\boldsymbol{\alpha}\right)^2 \\
&\quad = \sum_{n=1}^{N}\|\boldsymbol{\varphi}_n - (\mathbf{b}_n'\otimes\mathbf{K})\boldsymbol{\beta} - (\mathbf{b}_n'\otimes\mathbf{T})\boldsymbol{\alpha}\|_2^2 \\
&\quad = \|\boldsymbol{\varphi} - (\mathbf{B}\otimes\mathbf{K})\boldsymbol{\beta} - (\mathbf{B}\otimes\mathbf{T})\boldsymbol{\alpha}\|_2^2 .
\end{aligned}$$

Consider next the penalty term in the cost of (4). Substituting into (6), it follows that $\int_{\mathbb{R}^2}||\nabla^2\hat{g}_\nu(\boldsymbol{x})||_F^2 d\boldsymbol{x} = \boldsymbol{\beta}_\nu'\mathbf{K}\boldsymbol{\beta}_\nu$ [12, p. 33]. It thus holds that

$$\lambda\sum_{\nu=1}^{N_b}\int_{\mathbb{R}^2}||\nabla^2\hat{g}_\nu(\boldsymbol{x})||_F^2 d\boldsymbol{x} = \lambda\sum_{\nu=1}^{N_b}\boldsymbol{\beta}_\nu'\mathbf{K}\boldsymbol{\beta}_\nu = \lambda\boldsymbol{\beta}'(\mathbf{I}_{N_b}\otimes\mathbf{K})\boldsymbol{\beta}$$

from which (7) follows readily.

[1]The views and conclusions contained in this document are those of the authors and should not be interpreted as representing the official policies of the Army Research Laboratory or the U. S. Government.

REFERENCES

[1] A. Alaya-Feki, S. Ben Jemaa, B. Sayrac, P. Houze, and E. Moulines, "Informed spectrum usage in cognitive radio networks: Interference cartography," *Proc. of 19th Int. Symp. on Personal, Indoor and Mobile Radio Comms.,* Cannes, France, Aug. 31-Sep. 4, 2008.

[2] J.-A. Bazerque and G. B. Giannakis, "Distributed spectrum sensing for cognitive radio networks by exploiting sparsity," *IEEE Transactions on Signal Processing,* 2010 (to appear).

[3] J.-A. Bazerque, G. Mateos, and G. B. Giannakis, "Spline-based spectrum cartography for cognitive radio networks," *IEEE Transactions on Wireless Communications,* 2009 (submitted).

[4] J. Duchon, "Splines minimizing rotation-invariant semi-norms in Sobolev spaces," Springer-Verlag, Berlin, 1977.

[5] G. Ganesan, Y. Li, B. Bing, and S. Li, "Spatiotemporal sensing in cognitive radio networks," *IEEE Journal on Selected Areas in Communications,* vol. 26, no. 1, pp. 5-12, January 2006.

[6] T. Minka, "Old and new matrix algebra useful in statistics," Dec. 2000. [Online]. Available: http://research.microsoft.com/en-us/um/people/minka/papers/matrix/

[7] S. M. Mishra, A. Sahai, and R. W. Brodersen, "Cooperative sensing among cognitive radios," *Proc. of 42nd Intl. Conf. on Communications,* pp. 1658-1663, Istanbul, Turkey, June 11-15, 2006.

[8] K. Nishimori, R. Di Taranto, H. Yomo, P. Popovski, Y. Takatori, R. Prasad, and S. Kubota, "Spatial opportunity for cognitive radio systems with heterogeneous path loss conditions" *Proc. of 65th Vehicular Technology Conference,* pp. 2631-2635, Dublin, Ireland, April 22-25, 2007.

[9] Z. Quan, S. Cui, V. H. Poor, and A. H. Sayed, "Collaborative wideband sensing for cognitive radios," *IEEE Signal Processing Magazine*, vol. 25, no. 6, pp. 60-73, Nov. 2008.

[10] J. Riihijärvi, P. Mähönen, M. Wellens, and M. Gordziel, "Characterization and modelling of spectrum for dynamic spectrum access with spatial statistics and random fields," *Proc. of 19th Int. Symp. on Personal, Indoor and Mobile Radio Comms.,* Cannes, France, Aug. 31-Sep. 4, 2008.

[11] M. Unser, "Splines: A perfect fit for signal and image processing," *IEEE Signal Processing Magazine*, vol. 16, no. 6, pp. 22-38, Nov. 1999.

[12] G. Wahba, *Spline Models for Observational Data,* SIAM, Philadelphia, 1990.